Cerebral Cortex, April 2016;26: 1733–1746

doi: 10.1093/cercor/bhv007
Advance Access Publication Date: 30 January 2015
Original Article

ORIGINAL ARTICLE

Unmasking Language Lateralization in Human Brain Intrinsic Activity

Mark McAvoy[1], Anish Mitra[1], Rebecca S. Coalson[1,2], Giovanni d'Avossa[3], James L. Keidel[3], Steven E. Petersen[1,2,4,5,6,7], and Marcus E. Raichle[1,2,4,7]

[1]Department of Radiology, [2]Department of Neurology, Washington University, Saint Louis, MO 63110, USA, [3]School of Psychology, Bangor University, Bangor, UK, [4]Department of Anatomy and Neurobiology, [5]Department of Neurosurgery, [6]Department of Psychology and [7]Department of Biomedical Engineering, Washington University, Saint Louis, MO 63110, USA

Address correspondence to Mark McAvoy, Washington University School of Medicine, 4525 Scott Avenue, East Building, Room 2110, Campus Box, 8225, Saint Louis, MO 63110, USA. Email: mcavoy@npg.wustl.edu

Abstract

Lateralization of function is a fundamental feature of the human brain as exemplified by the left hemisphere dominance of language. Despite the prominence of lateralization in the lesion, split-brain and task-based fMRI literature, surprisingly little asymmetry has been revealed in the increasingly popular functional imaging studies of spontaneous fluctuations in the fMRI BOLD signal (so-called resting-state fMRI). Here, we show the global signal, an often discarded component of the BOLD signal in resting-state studies, reveals a leftward asymmetry that maps onto regions preferential for semantic processing in left frontal and temporal cortex and the right cerebellum and a rightward asymmetry that maps onto putative attention-related regions in right frontal, temporoparietal, and parietal cortex. Hemispheric asymmetries in the global signal resulted from amplitude modulation of the spontaneous fluctuations. To confirm these findings obtained from normal, healthy, right-handed subjects in the resting-state, we had them perform 2 semantic processing tasks: synonym and numerical magnitude judgment and sentence comprehension. In addition to establishing a new technique for studying lateralization through functional imaging of the resting-state, our findings shed new light on the physiology of the global brain signal.

Key words: attention network, global signal, hemispheric asymmetry, resting-state, semantic network

Introduction

Early postmortem lesion studies established the link between damage to left hemisphere inferior frontal and temporal cortical structures and pronounced language deficits (Broca 1861; Wernicke 1874). These early observations and many since from lesion (e.g., Damasio et al. 2004), split-brain (e.g., Gazzaniga 1983), and task-state functional imaging studies (for a review, see Price 2012) have revealed that the left hemisphere is specialized for language processing in the human brain. In contrast, results from resting-state functional imaging studies have been less clear. While one study showed left lateralization of both inferior frontal and temporal areas (Liu et al. 2009), others have failed to show left lateralization of temporal cortex (Smith et al. 2009), have instead showed right lateralization of inferior frontal areas (Tomasi and Volkow 2012), or have failed to show clear lateralization in either area (Lee et al. 2012; Hacker et al. 2013; Muller and Meyer 2014; Tie et al. 2014; Zhu et al. 2014). Thus, support for leftward lateralization of intrinsic activity in putative language processing areas has been conflicting.

The right hemisphere has been postulated to be specialized for attentional processing. Support comes from patients suffering from spatial neglect after right hemisphere damage (e.g., Heilman and Abell 1980), the performance of spatial tasks by split-brain individuals (e.g., LeDoux et al. 1977), and task-state functional imaging studies of visuospatial attention (e.g., Cai

et al. 2013). Regions commonly considered preferential for attentional processing include the frontal eye fields (FEFs) and intraparietal sulcus (IPS) of the dorsal attention system and the temporoparietal junction (TPJ) and ventral frontal/insular regions of the ventral attention system (for reviews, see Corbetta and Shulman 2011; Vossel et al. 2014). While resting-state imaging studies have found right ventral parietal regions to have greater functional connectivity to the ventral attention system than their left hemisphere homologs, the lateralization of parietal and frontal regions of the dorsal attention system has been much less clear (Fox et al. 2006; Hutchison et al. 2012; Kucyi et al. 2012; Lee et al. 2012; Daselaar et al. 2013; Hacker et al. 2013; Markett et al. 2014).

Previous work on the brain's lateralized organization in the resting-state has focused on the residual lateralization present after removal of the global signal (Liu et al. 2009; Gee et al. 2011; Wang et al. 2013). Although the global signal was originally regarded as a nuisance variable reflecting physiologic artifacts (Hampson et al. 2002; Greicius et al. 2003; Fox et al. 2005), its removal has been observed to change the topography among and relationship between systems (Weissenbacher et al. 2009) suggesting it includes a signal of neural origin (Scholvinck et al. 2010). We explored the hemispheric asymmetries in the resting-state global signal. Using a simple subtraction methodology that removed contributions from cardiac (Shmueli et al. 2007), respiration (Wise et al. 2004), and head movement signals (Power et al. 2012; Zeng et al. 2014) common to both hemispheres, we mapped the remaining neural signal over the entire brain to identify leftward and rightward asymmetric regions. We show hemispheric asymmetries of the global signal account for a substantial amount of variance and measure effect sizes. This mapping is found to be robust across models and is validated with a much larger data set. Finally, the functional relevance of these resting-state asymmetries was examined to identify regions preferential for semantic processing.

Materials and Methods

Paradigm and Subjects

Two fMRI data sets were analyzed. The first was a cohort of twenty healthy, right-handed subjects (8 male, average age 28.7) that participated in a resting and task-state experiment. The second was a previously published resting-state cohort of 120 healthy, young, right-handed subjects (60 male, average age 24.7) culled from 9 different studies (see Power et al. 2013 for details). This latter group was used to validate the resting-state effects found in the much smaller cohort. The Washington University Institutional Review Board approved the experimental protocols, and subjects gave written consent prior to participation.

For the smaller cohort, the resting and task-state experiment was completed in a single session and included 3 run types in the following order: 1) wakeful rest, 2) synonym and numerical magnitude judgment and 3) sentence comprehension. The experiment was performed in 3 series, so 3 runs of each type were collected. For the first run type, wakeful rest, subjects maintained fixation on a foveal crosshair for the duration of the 6-min run.

Synonym and numerical magnitude judgment tasks are used clinically to test verbal comprehension in semantic dementia and other aphasic groups (Lambon Ralph et al. 2009). For this second run type, we utilized a blocked design. For synonym judgment blocks, subjects indicated whether the second or third word was closer in meaning to the first. Likewise for numerical magnitude judgment blocks, subjects indicated whether the second or third number was closer in value to the first. Responses were made with a left-hand button press on an MR compatible button box. For both block types, blocks lasted 22.5 s and began with a foveal green crosshair for 2.5 s followed by 4 trials each with a duration of 5 s. The 3 individual stimuli within a trial were presented serially and foveally for 700 ms separated by a 250-ms blank interval. A 2.4-s response interval followed the third item. Blocks were randomized and separated by a 15-s fixation interval. Each 6.75-min run began and ended with a 15-s fixation interval and included 10 blocks, for a total of 30 blocks over the 3 runs. The first 8 subjects performed one version of this task, which included 15 synonym judgment blocks and 15 numerical magnitude judgment blocks. The remaining 12 subjects performed a second version with 20 synonym judgment blocks and 10 numerical magnitude judgment blocks. For this second version, the synonym judgment task included 10 blocks of abstract words (Coughlan and Warrington 1978; Warrington et al. 1998; Noppeney and Price 2004; Jefferies et al. 2009) and 10 blocks of sensory words (Noppeney and Price 2004).

For the third run type, sentence comprehension, subjects fixated on a foveal crosshair while listening to sentences through MR compatible headphones. Sentences were either plausible ("A broken wing meant the bird couldn't fly"), implausible ("A broken wing meant the bird couldn't write"), or spectrally rotated versions of implausible sentences. Spectrally rotated sentences were created by multiplying each implausible sentence by a 4500-Hz sine wave then low-pass filtering with a cutoff frequency of 4000 Hz (Scott et al. 2000). Spectral rotation retains some of the phonetics of normal speech, but intelligibility is very difficult (Blesser 1972). All sentences were normalized to have the same peak volume. Sentence presentation followed an event-related design, with each sentence lasting approximately 3 s followed by a randomly jittered interval to yield stimulus onset asynchronies of 5, 7.5 and 10 s. Each 5-min run included 13 sentences of each of the 3 types that were randomly intermixed. Thus, the entire experiment included 39 plausible, 39 implausible, and 39 rotated sentences. Passive sentence listening accesses speech comprehension, and the comparison of sentences with plausible and implausible meanings measures semantic processing while controlling for phonological, lexical, and syntactic processing along with working memory (Price 2010). The comparison of the sentences with plausible and implausible meanings to spectrally rotated sentences contrasts processing related to speech comprehension to more general auditory processing while controlling for the acoustic complexity and intonation structure of normal speech (Blesser 1972; Scott et al. 2000).

Stimulus Presentation

All stimuli were presented using E-Prime on a Dell laptop. Audio levels were set with a short trial run at the beginning of the experiment. Subjects listened to plausible, implausible, and spectrally rotated sentences and indicated with a button press whether the volume should be increased or decreased. The sentences presented during the trial run were different from the ones presented during the sentence comprehension task. For visual presentation a mirror was placed on the top of the head coil allowing visualization of stimuli on a projection screen via an LED projector at the back of the scanner.

Data Acquisition

Images were acquired with a Siemens 3 T Trio system (Erlangen) with a Siemens 12-channel Matrix head coil. A single high-

resolution structural run was acquired using a sagittal magnetization-prepared rapid gradient echo (MP-RAGE) sequence (slice echo time = 3.08 ms, TR = 2.4 s, inversion time = 1 s, flip angle = 8°, 176 slices, 1-mm isotropic voxels). Functional runs were acquired parallel to the anterior–posterior commissure using an asymmetric spin-echo echo-plana pulse sequence (TR = 2.5 s, T2 × evolution time = 27 ms, flip angle = 90°). Thirty-two contiguous interleaved 4-mm axial slices, with a 4 × 4 mm in-plane resolution, allowed for total brain coverage.

Image Preprocessing

Frame-by-frame movement correction data from the rotation and translation in the x, y, and z planes were computed for each participant for each run. Three runs had an overall movement of ≥1.5-mm RMS and were excluded from further analysis.

Image preprocessing included the following steps: 1) compensation for slice-dependent time shifts, 2) elimination of odd/even slice intensity differences due to interleaved acquisition, 3) realignment of all data acquired in each subject within and across runs to compensate for rigid body motion, and 4) normalization to a whole brain mode value of 1000 (Ojemann et al. 1997). The functional data were transformed into atlas space (Talairach and Tournoux 1988) by computing a sequence of affine transformations (first frame of BOLD run to T2-weighted fast spin-echo to MP-RAGE to atlas representative target), which were combined by matrix multiplication, resampling to a 2-mm isotropic grid. For cross-modal (i.e., functional to structural) image registration, a locally developed algorithm was used (Rowland et al. 2005).

Wakeful Rest: Modeling Hemispheric Asymmetries of the Global BOLD Signal

To examine lateralized differences of the resting-state global signal, we considered 2 models: a hemispheric model in which weights were estimated for each hemisphere and a differential model that estimated asymmetric and symmetric weights.

The hemispheric model

The hemispheric model is motivated by the structure of the brain with its 2 hemispheres that are approximately mirror images (Keller et al. 2009). Subject-specific general linear models (GLMs) (Friston et al. 1995) were fit to the BOLD time series at each voxel:

$$\begin{aligned}\mathrm{BOLD}_j(t) = {} & L_{\mathrm{global}j} l_{\mathrm{global}j}(t) + R_{\mathrm{global}j} r_{\mathrm{global}j}(t) + L_{\mathrm{WM}j} l_{\mathrm{WM}j}(t) \\ & + R_{\mathrm{WM}j} r_{\mathrm{WM}j}(t) + L_{\mathrm{CSF}j} l_{\mathrm{CSF}j}(t) + R_{\mathrm{CSF}j} r_{\mathrm{CSF}j}(t) \\ & + \mathrm{MOTION}_j \mathrm{motion}_j(t) + \mathrm{LPF}_j \mathrm{lpf}_j(t) + c_{0j} + c_{1j} t\end{aligned} \quad (1)$$

where $l_{\mathrm{global}j}(t)$ and $r_{\mathrm{global}j}(t)$ are the time series of the left and right hemispheres for the jth run, which were formed by removing the linear trend and intercept at the voxel level then averaging over all voxels in the left and right hemispheres, respectively. Similarly, $l_{\mathrm{WM}j}(t)$, $r_{\mathrm{WM}j}(t)$ and $l_{\mathrm{CSF}j}(t)$, $r_{\mathrm{CSF}j}(t)$ are the time series of white matter and ventricular signals, respectively. These regressors were formed from each individual's eroded white matter and ventricular masks (e.g., Power et al. 2014) by removing the linear trend and intercept at each voxel then averaging over the left and right hemisphere voxels, respectively. Head movement signals were accounted for by $\mathrm{motion}_j(t)$ which represents 24 time series formed from measured head shifts and angular displacements in 3 dimensions (i.e., X, Y, Z, pitch, yaw, and roll) along with their squares, derivatives, and squared derivatives (Friston et al. 1996; Satterthwaite et al. 2013; Yan et al. 2013; Power et al. 2014). The low-pass filter $\mathrm{lpf}_j(t)$ was implemented with a Fourier basis set that consisted of sine and cosine pairs modeling full cycles from the cutoff of 0.08 Hz (Biswal et al. 1995; Lowe et al. 1998) to the Nyquist frequency (e.g., McAvoy et al. 2008). Additional terms included the constant c_0 and linear trend $c_1 t$ to remove slow drifts in the time series. Solving the partial correlation model of Equation 1 via ordinary least squares yielded estimates of the left and right hemisphere global signal weights, $L_{\mathrm{global}j}$ and $R_{\mathrm{global}j}$. Importantly, each voxel from each hemisphere was estimated independently in Equation 1. Homotopic voxels were not paired, rather components $L_{\mathrm{global}j} l_{\mathrm{global}j}(t)$ and $R_{\mathrm{global}j} r_{\mathrm{global}j}(t)$ extracted the left and right hemisphere global signal contributions to the resting-state time series $\mathrm{BOLD}_j(t)$ of each voxel.

The estimated weights L_{global} and R_{global} were normalized by the constant term averaged over runs, then spatially smoothed with a 4-mm full width at half maximum (FWHM) 3D gaussian kernel to blur individual differences in brain anatomy. Statistical significance was assessed with a group-level two-tailed, paired Student's T-test on the difference between left and right hemisphere weights. The statistical map was z-transformed and corrected for multiple comparisons ($|z| \geq 3.0$, minimum 21 face-connected voxels, $P < 0.05$ corrected) with a Monte Carlo-based method (Forman et al. 1995; McAvoy et al. 2001).

The differential model

The hemispheric model estimates weights for each hemisphere but does not directly estimate the asymmetric and symmetric weightings between hemispheres. To extract these weights, subject-specific GLMs were fit to the BOLD time series at each voxel:

$$\begin{aligned}\mathrm{BOLD}_j(t) = {} & \mathrm{ASYM}_{\mathrm{global}j}[l_{\mathrm{global}j}(t) - r_{\mathrm{global}j}(t)] + \mathrm{SYM}_{\mathrm{global}j}[l_{\mathrm{global}j}(t) \\ & + r_{\mathrm{global}j}(t)] + \mathrm{ASYM}_{\mathrm{WM}j}[l_{\mathrm{WM}j}(t) - r_{\mathrm{WM}j}(t)] + \mathrm{SYM}_{\mathrm{WM}j}[l_{\mathrm{WM}j}(t) \\ & + r_{\mathrm{WM}j}(t)] + \mathrm{ASYM}_{\mathrm{CSF}j}[l_{\mathrm{CSF}j}(t) - r_{\mathrm{CSF}j}(t)] + \mathrm{SYM}_{\mathrm{CSF}j}[l_{\mathrm{CSF}j}(t) \\ & + r_{\mathrm{CSF}j}(t)] + \mathrm{MOTION}_j \mathrm{motion}_j(t) + \mathrm{LPF}_j \mathrm{lpf}_j(t) + c_{0j} + c_{1j} t\end{aligned} \quad (2)$$

where $l_j(t)$ and $r_j(t)$ are the time series of the left and right hemispheres for the jth run, which were formed by removing the linear trend and intercept at the voxel level then averaging over all left or right hemisphere voxels for the global signal or the respective eroded masks for the white matter and ventricular signals. The regressor modeling the asymmetric signal $[l_j(t) - r_j(t)]$ and the regressor modeling the symmetric signal $[l_j(t) + r_j(t)]$ were normalized to their RMS values (i.e., standard deviation). This effectively implements a z-score normalization, ensuring equivalent loadings in the model. Without this normalization, the loadings on the asymmetric weights would be biased to be disproportionally larger than that on the symmetric weights. This is best understood by examining Figure 1, in that the sum of the left and right hemisphere time series (blue and red traces, respectively) will be a regressor with very large fluctuations compared with the difference. Additional terms included head motion $\mathrm{motion}_j(t)$, the low pass filter $\mathrm{lpf}_j(t)$, constant c_0 and linear trend $c_1 t$. See "hemispheric model" above for details. Solving the partial correlation model of Equation 2 via ordinary least squares parsed the global signal into asymmetric $\mathrm{ASYM}_{\mathrm{global}j}$ and symmetric $\mathrm{SYM}_{\mathrm{global}j}$ weights. Once again homotopic voxels were not paired, rather the component $\mathrm{ASYM}_{\mathrm{global}j}[l_{\mathrm{global}j}(t) - r_{\mathrm{global}j}(t)]$ extracted the lateralized contribution and $\mathrm{ASYM}_{\mathrm{global}j}[l_{\mathrm{global}j}(t) + r_{\mathrm{global}j}(t)]$ extracted the common contribution across hemispheres of the global signal to the resting-state time series $\mathrm{BOLD}_j(t)$ of each voxel.

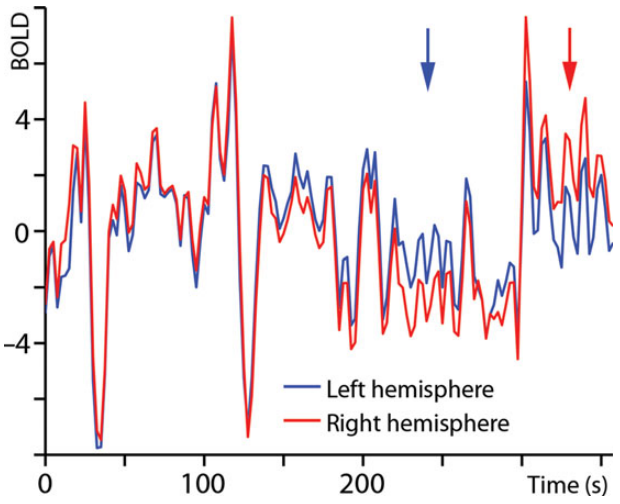

Figure 1. Left and right hemisphere time series of a single subject during wakeful rest. Shown is an entire 6-min fixation run. Time series are averaged over all voxels in the respective hemisphere. These are examples of the time series $l_{global}(t)$ and $r_{global}(t)$ for the left and right hemisphere, respectively, used to estimate the global signal weights in Equations 1 and 2 (see Materials and Methods). The blue arrow points to an epoch where the spontaneous fluctuations of the left hemisphere exceed the right. The red arrow points to an epoch where the spontaneous fluctuations of the right hemisphere exceed the left. These amplitude fluctuations occur without a change in phase between hemispheres.

The estimated weight $ASYM_{global}$ was normalized by the constant term averaged over runs, then spatially smoothed with a 4-mm FWHM 3D gaussian kernel to blur individual differences in brain anatomy. Statistical significance was assessed with a group-level two-tailed, one-sample Student's *T*-test. The statistical map was z-transformed and corrected for multiple comparisons ($|z| \geq 3.0$, minimum 21 face-connected voxels, $P < 0.05$ corrected) with a Monte Carlo-based method (Forman et al. 1995; McAvoy et al. 2001).

Analysis: Synonym and Numerical Magnitude Judgment

Subject-specific GLMs estimated the evoked BOLD response time-locked to the green crosshair cueing the start of a trial block. The GLM regressors included 2 sets of delta functions, one for synonym judgment blocks and the other for the numerical magnitude blocks, each modeling the BOLD response over 15 timepoints. Additional regressors included a constant term and linear trend for each run. The estimated responses were normalized by the value of the constant term averaged over runs, then spatially smoothed with a 4-mm FWHM 3D gaussian kernel. Statistical significance was assessed with a group-level repeated-measures analysis of variance (ANOVA) with subjects as the random factor and 2 fixed factors (e.g., Keppel 1991): block type (synonym and numerical magnitude) and time (15 timepoints). The resulting statistical maps, which included the task by time interaction ($F_{14,266}$), were sphericity-corrected (Algina 1997), z-transformed and corrected for multiple comparisons ($|z| \geq 3.0$, minimum 45 face-connected voxels, $P < 0.05$ corrected) with a Monte Carlo-based method (Forman et al. 1995; McAvoy et al. 2001).

Analysis: Sentence Comprehension

Subject-specific GLMs estimated the evoked BOLD response time-locked to the start of each plausible, implausible, and spectrally rotated sentence. Regressors included 3 sets of delta functions, one for each sentence type, each modeling the BOLD response over 10 timepoints. Additional regressors included a constant term and linear trend for each run. The estimated responses were normalized by the value of the constant term averaged over runs, then spatially smoothed with a 4-mm FWHM 3D gaussian kernel. Statistical significance was assessed with a group-level repeated-measures ANOVA with subjects as the random factor and 2 fixed factors: sentence type (plausible, implausible, and rotated) and time (10 timepoints). The resulting statistical maps, which included the sentence type by time interaction ($F_{9,171}$), were sphericity-corrected (Algina 1997), z-transformed, and corrected for multiple comparisons ($|z| \geq 3.0$, minimum 45 face-connected voxels, $P < 0.05$ corrected) with a Monte Carlo-based method (Forman et al. 1995; McAvoy et al. 2001).

Results

Hemispheric Asymmetries of the Resting-State Global Signal

Plotted in Figure 1 are examples of the hemispheric time series $l_{globalj}(t)$ and $r_{global}(t)$ from a single run of a single subject. Although the 2 time series are in phase, the amplitude of the spontaneous fluctuations between the 2 hemispheres waxes and wanes such that for some epochs the left hemisphere dominates, while other epochs are dominated by the right hemisphere. Our null hypothesis is that these amplitude modulations are within the noise of the BOLD signal. This null hypothesis was tested voxelwise across the entire brain with a group-level paired Student's *T*-test (see Materials and Methods) demonstrating that statistically significant differences exist in many cortical areas. In Figure 2, regions shown in hot colors displayed a significant leftward asymmetry characterized by a left global weight (L_{global}, Eq. 1) that was greater than the right (R_{global}). Regions shown in cool colors displayed a significant rightward asymmetry characterized by a right global weight that was greater than the left. MNI152 coordinates are reported in Table 1. Areas in the left hemisphere with a leftward asymmetry included a broad swath of regions along the precentral gyrus extending into the precentral sulcus (dPreC, larynx, and tongue cortex, c.f. Brown et al. 2008), extending anteriorly onto the inferior frontal gyrus (dpOp and vpOp), extending into the inferior frontal sulcus and onto the middle frontal gyrus (MFG), and dorsally into the superior frontal sulcus and onto the superior frontal gyrus (SFG). In temporal cortex, regions along the posterior superior temporal sulcus (pSTS) are highlighted with additional regions along the middle temporal gyrus (MTG), extending dorsally onto the superior temporal gyrus and ventrally into inferotemporal cortex (VWFA, c.f. Petersen et al. 1990; Cohen and Dahaene 2004). In posterior parietal cortex, shown are regions along the angular gyrus (AG) extending into the inferior parietal lobe (IPL). On the mesial surface regions were found in dorsal medial prefrontal cortex, precuneus and along the collateral sulcus, and the caudate subcortically (data not shown). The cerebellum was the only right hemisphere area to display a leftward asymmetry with regions in Crus I and II (Figure 4A, third column and Table 1, c.f. Petersen et al. 1989; Wang et al. 2013).

With the exception of the cerebellum, significant areas in the right hemisphere displayed a rightward asymmetry including regions along the supramarginal gyrus (vSMG), extending posteriorly onto the AG, dorsally into the IPS and ventrally into TPJ. These latter 2 posterior parietal regions (IPS and TPJ) along with the FEFs

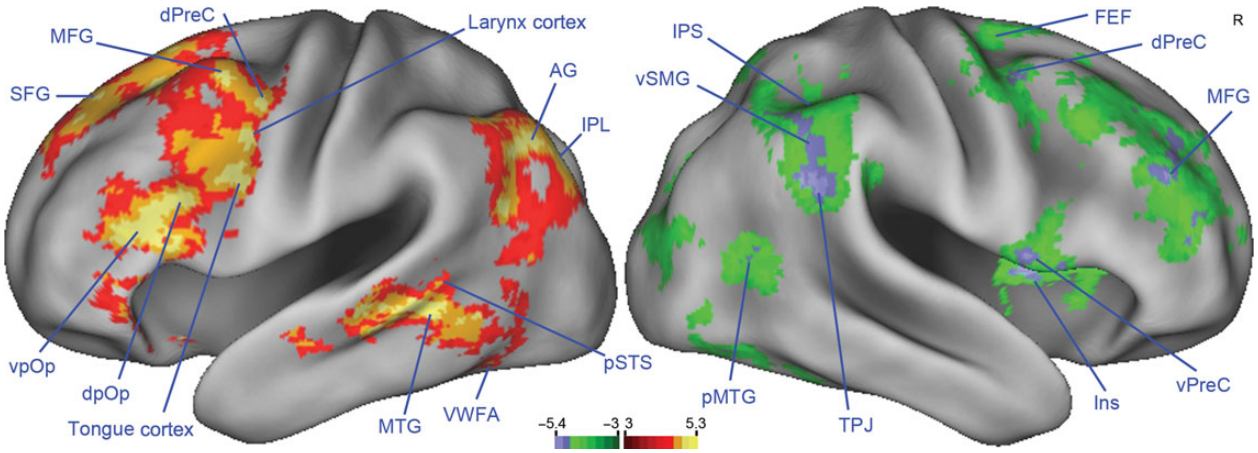

Figure 2. Hemispheric asymmetries of the resting-state global signal. Group-level statistical map of the difference between left and right global weights (L_{global} and R_{global}, Eq. 1) during wakeful rest. Regions shown in hot colors display a significant leftward asymmetry, whereas regions shown in cool colors display a significant rightward asymmetry. Shown on the inflated lateral cortical surface are gaussianized T statistics from a Student's paired *T*-test corrected for multiple comparisons ($P < 0.05$). Peak coordinates and abbreviations are listed in Table 1. In the left hemisphere, many putative language processing areas are identified including regions along the inferior frontal gyrus (dpOp) and superior temporal sulcus (pSTS). In the right hemisphere, many putative attention processing areas are identified including regions in frontal cortex (FEF), along the IPS and the TPJ.

Table 1 Coordinates of regions with significant differences in left and right global components as identified in Figures 2 and 4A

Region[a]	Abbreviation	Peak[b]			Volume	$ASYM_{global}$	SYM_{global}	Differential ratio
		x	y	z	mm^3	$R^2 \pm sem^c$	$R^2 \pm sem^c$	$ASYM_{global}/SYM_{global}$
Left MFG	LMFG	−46	9	53	416	0.065 ± 0.007	0.130 ± 0.019	0.50
Left MTG	LMTG	−64	−38	1	464	0.063 ± 0.008	0.169 ± 0.023	0.37
Left SFG	LSFG	−25	37	49	632	0.074 ± 0.009	0.094 ± 0.016	0.79
Left dorsal pars opercularis	LdpOp	−49	19	25	408	0.072 ± 0.009	0.120 ± 0.018	0.60
Left precentral cortex	Larynx	−46	5	36	360	0.060 ± 0.007	0.118 ± 0.018	0.51
Left dorsal precentral cortex	LdPreC	−44	3	47	368	0.063 ± 0.009	0.160 ± 0.020	0.39
Left IPL	LIPL	−36	−71	42	400	0.068 ± 0.008	0.122 ± 0.014	0.56
Left ventral pars opercularis	LvpOp	−42	36	11	432	0.053 ± 0.006	0.077 ± 0.013	0.69
Left pSTS	LpSTS	−54	−42	1	656	0.054 ± 0.007	0.145 ± 0.021	0.37
Left AG	LAG	−36	−71	44	360	0.059 ± 0.006	0.129 ± 0.015	0.46
Left precentral cortex	Tongue	−49	9	27	344	0.052 ± 0.005	0.103 ± 0.015	0.50
Left inferotemporal cortex	VWFA	−46	−55	−13	336	0.038 ± 0.005	0.189 ± 0.020	0.20
Right lateral inferior cerebellum, Crus I	RCBI	29	−76	−35	368	0.037 ± 0.005	0.108 ± 0.011	0.34
Right posterior cerebellum, Crus II	RCBII	17	−76	−26	200	0.044 ± 0.005	0.094 ± 0.011	0.46
Right posterior MTG	RpMTG	49	−56	12	328	0.040 ± 0.004	0.151 ± 0.016	0.27
Right IPS	RIPS	44	−45	45	440	0.055 ± 0.007	0.116 ± 0.012	0.47
Right dorsal precentral cortex	RdPreC	42	6	49	432	0.046 ± 0.004	0.161 ± 0.017	0.29
Right insula	RIns	41	5	2	352	0.051 ± 0.006	0.126 ± 0.017	0.41
Right TPJ	RTPJ	60	−40	28	448	0.062 ± 0.005	0.138 ± 0.015	0.45
Right MFG	RMFG	42	45	21	368	0.065 ± 0.008	0.122 ± 0.020	0.53
Right FEF	RFEF	26	0	64	496	0.054 ± 0.007	0.148 ± 0.021	0.37
Right ventral supramarginal gyrus	RvSMG	61	−42	39	336	0.086 ± 0.009	0.123 ± 0.013	0.70
Right ventral precentral cortex	RvPreC	62	12	−1	328	0.062 ± 0.007	0.201 ± 0.023	0.31

[a]All regions were hand drawn on the peaks of the statistical image shown in Figures 2 and 4A.
[b]Peak coordinates are given in millimeters according to the MNI152 atlas.
[c]R^2 is the amount of variance accounted for by the respective component from the differential model averaged across the twenty subjects (see Eq. 2, Materials and Methods).

have been implicated in attentional processing (for reviews, see Corbetta and Shulman 2011; Vossel et al. 2014). Regions are also found in posterior temporal (pMTG), inferotemporal and parieto-occipital cortex. In the anterior brain, a broad swath of regions is found along the MFG extending into the superior frontal sulcus. Additional regions are found dorsally along the precentral sulcus (dPreC) extending onto the central gyrus and ventrally (vPreC) extending into the insula (Ins). These latter regions in the middle and posterior (data not shown) insula have been identified to emotional processing (Duerden et al. 2013). On the mesial surface, regions are found along the SFG, precuneus, parieto-occipital sulcus, and the fusiform gyrus extending into the collateral sulcus, as well as subcortically in dorsomedial and posterior thalamic nuclei (data not shown).

Omitting frames of the BOLD time series with a framewise displacement (Power et al. 2012) of >0.2 mm, the current recommendation for normal adult subjects (Power et al. 2014) yielded a map similar to that shown in Figure 2 (data not shown). The group-level paired Student's *T*-test of the difference between L_{WM} and R_{WM} yielded regions largely confined to the white matter (data not shown). Likewise, the group-level paired Student's *T*-test of the difference between L_{CSF} and R_{CSF} yielded regions largely confined to the ventricles (data not shown).

Variance Explained and Effect Sizes of Hemispheric Asymmetries

Although Figure 2 is a statistically significant map corrected for multiple comparisons, it is possible that these global signal asymmetries account for little variance in the spontaneous fluctuations. Table 1 reports the R^2 values of the asymmetric ($ASYM_{global}$) and symmetric (SYM_{global}) weights from the differential model (Eq. 2) for each region averaged across the twenty subjects. Altogether the combined R^2 of the asymmetric and symmetric weights averaged across the 23 regions was 0.18 ± 0.028, thus explaining 18% of the variance in the BOLD time series, in line with other estimates of the variance accounted for by the global signal (Carbonell et al. 2011). We also wished to ascertain how much variance the asymmetric weight explained relative to the symmetric. This differential ratio is found in the last column of Table 1 and is the variance explained by the asymmetric weight divided by the variance explained by the symmetric weight ($R^2_{ASYM_{global}}/R^2_{SYM_{global}}$). Values ranged from 0.20 to 0.79 (mean = 0.46).

Having established that global signal hemispheric asymmetries explain a significant amount of variance in the brain's spontaneous fluctuations, we next examined effect sizes. Shown in the top panel of Figure 3 are the subject averaged L_{global}- and R_{global} weights extracted from the hemispheric model of Equation 1. Shown in the bottom panel are the subject averaged $ASYM_{global}$ and SYM_{global} weights extracted from the differential model of Equation 2. Displayed units are percent BOLD signal computed for each subject by normalizing to the value of the constant term averaged over runs, multiplying by 100 then taking the mean across subjects. Coordinates of plotted regions are provided in Table 1. Considering first just the top panel, a leftward asymmetric region is defined as having a larger positive L_{global} weight and a smaller negative R_{global} weight (e.g., LMFG), whereas a rightward asymmetric region is defined as having a larger positive R_{global} weight and a smaller negative L_{global} weight (e.g., RvPreC). As a basis for comparison, 2 contralateral homologs that lacked a significant differential relation between left and right hemisphere spontaneous fluctuations were defined as 10-mm-diameter spheres at Talairach coordinates (–10, –90, and 0) and (10, –90, and 0) (MNI coordinates: [–11, –91, and 3], [10, –91, and 2]), located in left and right primary visual cortex (LV1 and RV1). These 2 regions had a very different pattern. LV1 had positive L_{global} and R_{global} weights of equal amplitude, whereas RV1 had a larger positive R_{global} weight and a smaller positive L_{global} weight. The group averaged R^2 values of LV1 and RV1 over L_{global} and R_{global} weights were 0.20 ± 0.013 and 0.28 ± 0.026, respectively, whereas the mean over the 23 regions with significant hemispheric asymmetries was 0.18 ± 0.028. Thus, the lack of an asymmetrical relationship did not result from poor fit of the model expressed in Equation 1. Rather these non-asymmetrical and statistically nonsignificant patterns in bilateral visual cortex may be explained by the observation that in homotopic

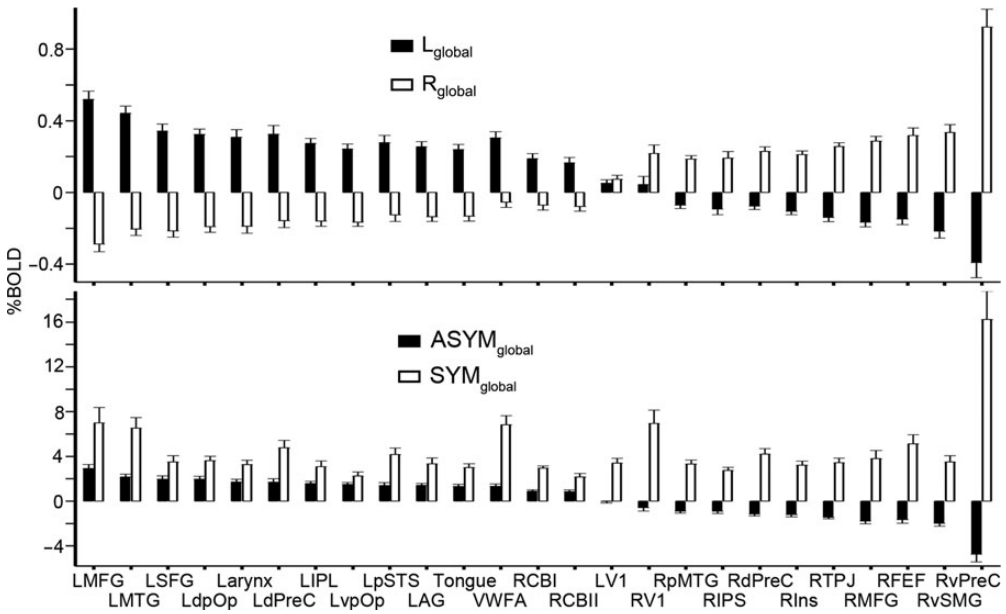

Figure 3. Resting-state global signal asymmetries show a complementary relationship between hemispheres. Group averaged left and right global weights from the hemispheric model (Eq. 1, Materials and Methods) and asymmetric and symmetric weights from the differential model (Eq. 2, Materials and Methods). Coordinates are provided in Table 1. Top panel. Regions with a leftward asymmetry had a larger positive L_{global} weight and a smaller negative R_{global} weight, whereas regions with a rightward asymmetry had a larger positive R_{global} weight and a smaller negative L_{global} weight. The right cerebellum (RCBI and RCBII) shows a leftward asymmetry in contrast to the other right hemisphere regions. Left and right visual cortex (LV1 and RV1) were defined as 10-mm-diameter spheres centered at Talairach coordinates (–10, –90, and 0) and (10, –90, and 0) (MNI coordinates: [–11, –91, and 3] and [10, –91, and 2]), respectively. They provide a basis for comparison as visual cortex did not show hemispheric asymmetries (see Fig. 4*A*,*B*, axial slice *Z* = 0). While regions that displayed hemispheric asymmetries had a sign change between L_{global} and R_{global} components, both components were positive for LV1 and RV1. Bottom panel. Leftward asymmetric regions had a positive $ASYM_{global}$ weight, and rightward asymmetric regions had a negative $ASYM_{global}$ weight. Percent BOLD signal was computed for each subject by normalizing to the value of the constant term averaged over runs, then multiplying by 100. Displayed are the mean percentages across subjects.

regions, intrahemispheric signals are more correlated than interhemispheric signals (Gee et al. 2011). The pattern between left and right global weights in the remaining regions supports the notion of a complementary relationship between hemispheres (Sperry 1982).

Considering now the bottom panel of Figure 3, a leftward asymmetric region (e.g., LMFG) had a positive asymmetric weight ($ASYM_{global}$), whereas a rightward asymmetric region (e.g., RvPreC) has a negative asymmetric weight. Normalization of the differential model regressors resulted in much larger weights than those extracted from the hemispheric model shown in the top panel (see Materials and Methods), but our interest is the ratio of asymmetric to symmetric weightings. Regions with a leftward asymmetry had ratios that ranged from 0.19 to 0.66, whereas rightward asymmetric regions had ratios that ranged from −0.27 to −0.56. The ratios for LV1 and RV1 were −0.008 and −0.085. In summary, we found that effect sizes were consistent with measures of explained variance, in that regions with significant global signal hemispheric asymmetries had an asymmetric weighting that was on average 40% (mean of the 23 regions) that of the symmetric weighting, and this asymmetric weighting accounted for 46% of the variance relative to the symmetric weighting.

Robustness of Hemispheric Asymmetries across Models and Data Sets

The differential model assessed hemispheric asymmetries with a single weight ($ASYM_{global}$, Eq. 2). The one-sample Student's *T*-test of this weight produced a very similar map to that of the paired Student's *T*-test between L_{global} and R_{global} weights extracted from the hemispheric model (Eq. 1) as seen by comparing Figure 4*B* with *A*. We validated this mapping with a second, larger resting-state data set of 120 subjects (see Materials and Methods). Figure 4*E* shows the difference between L_{global} and R_{global} weights from a paired Student's *T*-test on this cohort. Comparing this map to the smaller cohort of Figure 4A, we find good anatomical correspondence between peak areas.

Leftward Asymmetric Regions in Left Frontal and Temporal Cortex and the Right Cerebellum are Preferential for Semantic Processing

Although hemispheric asymmetries of the global spontaneous fluctuations uncovered many regions long regarded as important for language processing including regions along the inferior frontal gyrus (Bookheimer 2002), superior temporal sulcus (Wise et al. 2001), and the right cerebellum (Petersen et al. 1989; Fiez et al. 1992), we sought to confirm the anatomical correspondence of the task-state. Shown in Figure 4A,*B* are hemispheric asymmetries in the resting-state global signal for the hemispheric and differential models, respectively. Shown in Figure 4C is the interaction of block type by time highlighting regions whose BOLD responses were modulated over time between the synonym judgment and numerical magnitude task. This map is signed with mean of the response evoked for synonym judgments minus the mean of the response evoked for numerical magnitude judgments. Thus, regions with larger BOLD responses to synonym blocks are shown in hot colors, and regions with larger responses to number blocks are shown in cool colors. Shown in Figure 4D is the interaction of sentence type by time highlighting regions whose BOLD responses were modulated over time by the plausible, implausible, and spectrally rotated sentences. In

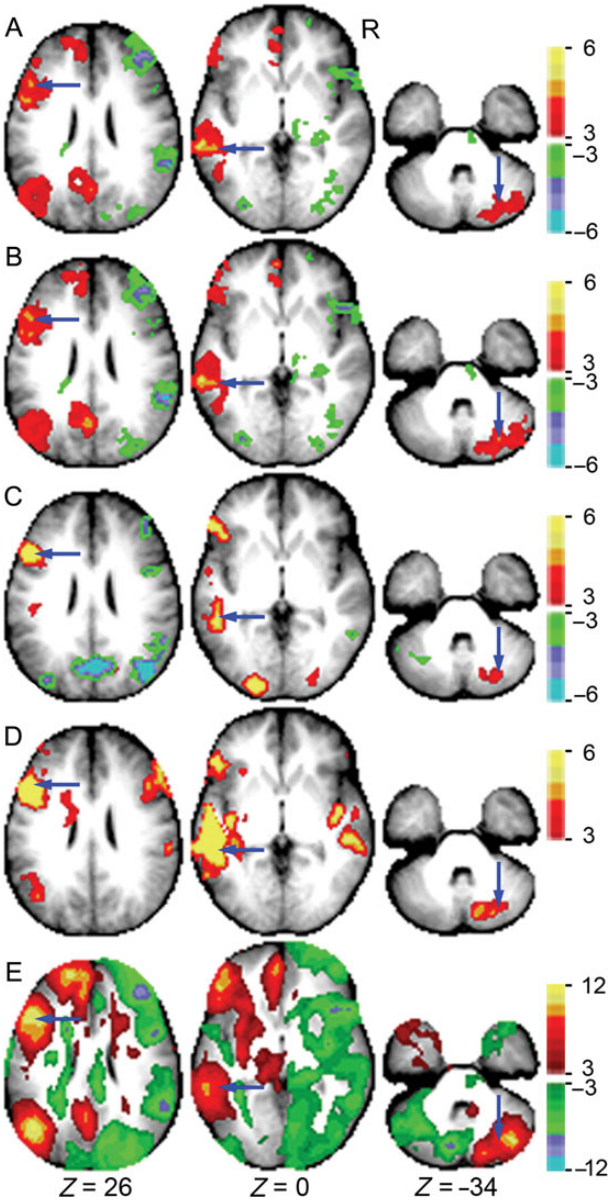

Figure 4. Group-level statistical maps highlighting the robustness of resting-state global signal hemispheric asymmetries across models (*A*,*B*), anatomical correspondence with language tasks (*C*,*D*) and validation with a second, larger data set (*E*). (*A*) Hemispheric asymmetries of the resting-state global signal as estimated by the hemispheric model (Eq. 1, Materials and Methods). Shown is a paired Student's *T*-test on the difference between L_{global} and R_{global} weights. The 3 axial slices are taken from the same map shown in Figure 2. (*B*) Hemispheric asymmetries of the resting-state global signal as estimated by the differential model (Eq. 2, Materials and Methods). Shown is a one-sample Student's *T*-test on the asymmetric weight. (*C*) Synonym and numerical magnitude judgment task. Shown is the interaction of block type by time highlighting regions whose BOLD responses differentiated between the synonym and number blocks. This map is signed with the mean difference of the 2 blocks (synonyms—numbers). (*D*) Sentence comprehension task. Shown is the interaction of sentence type by time highlighting regions whose BOLD responses differentiated between plausible, implausible, and spectrally rotated sentences. (*E*) 120 subject validation data set. Hemispheric asymmetries of the resting-state global signal as estimated by the hemispheric model. Shown is a paired Student's *T*-test on the difference between L_{global} and R_{global} weights. Displayed values in (*A*,*B*) and (*E*) are gaussianized T statistics; (*C*,*D*) are gaussianized *F* statistics. All maps have been corrected for multiple comparisons ($P < 0.05$). Three regions are identified with blue arrows: left dorsal pars opercularis in the first column, LpSTS in the second column, and the RCBI in the third column. See Table 1 for coordinates.

the first column, the left dorsal pars opercularis (LdpOp), in the second column the left posterior superior temporal sulcus (LpSTS), and in the third column the right lateral inferior cerebellum (RCBI) are identified. We may conclude that regions identified from hemispheric asymmetries in the resting-state global signal have good anatomical correspondence to regions preferential for sematic processing.

Having established initial face validity, we further examined these regions across both tasks with direct post hoc statistical comparisons. It is quite possible that voxelwise differences between synonym and numerical magnitude shown in Figure 4C are driven purely by reaction time and accuracy differences. It is also possible that none of the regions discriminate between the abstract and sensory word blocks. Reaction times and accuracy were recorded for 11 of the 12 subjects that performed the second version of this task that included the 3 different block types (abstract, sensory, and number). A repeated-measures ANOVA with subjects as the random factor and reaction time as the fixed factor found no significant difference between the 3 types of blocks ($F_{2,20} = 0.86$, $P = 0.44$). Mean reaction times for the abstract, sensory, and number blocks were 1043 ± 91, 1001 ± 87, and 992 ± 95 ms, respectively. However, the repeated-measures ANOVA performed on accuracy was significant ($F_{2,20} = 4.88$, $P = 0.02$). Mean accuracies for the abstract, sensory, and number blocks were $90.05 \pm 5.50\%$, $94.43 \pm 4.16\%$, and $94.09 \pm 4.07\%$, respectively. Post hoc tests confirmed the significance of the lower accuracy for synonym judgments on abstract words (abstract vs. sensory: $F_{1,10} = 5.43$, $P = 0.04$; abstract vs. number: $F_{1,10} = 10.19$, $P = 0.0096$).

The evoked BOLD responses of the 12 subjects that performed the second version of the synonym and numerical magnitude judgment task with 3 different block types were analyzed with 2 post hoc repeated-measures ANOVAs. The random factor was subjects with fixed factors of block type and time (15 timepoints). In the first, block type was analyzed at 3 levels (abstract, sensory, and number) to determine if the evoked response distinguished between the 3 block types. If the interaction of block type by time was significant, then a second ANOVA with block type at 2 levels (abstract and sensory) was performed to test whether the region distinguished between abstract and sensory words. Results from the former ANOVA with block type at 3 levels are shown in the second column of Table 2 and those from the latter with block type at 2 levels are shown in the third column. A region was given a stimulus preference as indicated in the fourth column, if its BOLD response differentiated between abstract, sensory, and number blocks. If the response was greater for numbers, then this indicated a number preference. Likewise, if the response was greater for either abstract or sensory words, then this indicated a word preference. If the region's response differentiated between abstract and sensory blocks, then this latter distinction was refined to a stimulus preference for either abstract or sensory blocks depending on which response was larger. As indicated in Table 2, the right cerebellum (RCBI and RCBII) was the only right hemisphere area with a word preference. All left hemisphere regions except for those in parietal cortex (LAG) had a word preference with the superior frontal gyrus (LSFG), dorsal pars opercularis (LdpOp), pSTS, and the RCBI having a preference for abstract words, though this may reflect the lower accuracy of

Table 2 Statistics of regions identified in Table 1 for the two language tasks

Region	Synonym and numerical magnitude judgment			Sentence comprehension		
	Interaction of block type by time			Interaction of sentence type by time		
	Abstract vs. sensory vs. number *P*-value	Abstract vs. sensory[b] *P*-value	Stimulus preference[a]	Plausible vs. implausible vs. rotated *P*-value	Plausible vs. implausible[c] *P*-value	Stimulus preference[a]
LMFG	0.565			3.72e − 9	0.0577	Normal
LMTG	0.333			2.33e − 11	0.00836	Implausible
LSFG	0.0206	0.00425	Abstract	0.854		
LdpOp	1.63e − 15	0.0163	Abstract	3.24e − 30	1.59e − 9	Implausible
Larynx	0.429			1.33e − 12	0.000787	Implausible
LdPreC	0.0792			1.33e − 17	0.147	Normal
LIPL	0.297			0.00392	0.552	Normal
LvpOp	0.000804	0.679	Words	8.37e − 8	0.00654	Implausible
LpSTS	1.89e − 9	0.0119	Abstract	4.73e − 41	4.90e − 5	Implausible
LAG	0.000185	0.374	Numbers	0.190		
Tongue	0.0338	0.507	Words	4.82e − 10	0.000106	Implausible
VWFA	0.597			0.000615	0.458	Normal
RCBI	3.43e − 6	0.0199	Abstract	1.00e − 6	0.000948	Implausible
RCBII	4.40e − 5	0.654	Words	1.48e − 9	0.000860	Implausible
RpMTG	0.166			0.0699		
RIPS	3.23e − 16	0.172	Numbers	0.820		
RdPreC	0.000162	0.00560	Numbers	0.419		
RIns	0.792			0.0864		
RTPJ	0.00187	0.913	Numbers	0.00309	0.720	Rotated
RMFG	0.000209	0.0764	Numbers	0.0807		
RFEF	0.000203	0.283	Numbers	0.193		
RvSMG	1.28e − 8	0.474	Numbers	0.00131	0.421	Rotated
RvPreC	0.795			0.115		

[a]Stimulus with the largest evoked BOLD response.
[b]If this interaction is not significant, then the region will have a preference for either words or numbers.
[c]If this interaction is not significant, then the regions will have a preference for either normal or rotated speech.

the synonym judgment on abstract items. We next sought to confirm this left hemisphere preference for semantic processing by comparing the evoked responses from contralateral homologs of the latter 3 regions. These contralateral regions (RdpOp, RpSTS, and LCBI) were created by changing the sign of the *X* coordinate shown in Table 1, then drawing a 10-mm-diameter sphere at that point. Comparing the regions pairwise in the first column of Figure 5, we see that the evoked responses of the contralateral homologs fail to distinguish abstract and sensory blocks from the number blocks.

For the sentence comprehension task, it is quite possible that the voxelwise interaction of sentence type by time shown in Figure 4*D* is driven purely by the difference between intelligible (i.e., plausible and implausible sentences) and unintelligible speech. To investigate this possible confound, the analysis paralleled that performed on the synonym and numerical magnitude judgment task with 2 post hoc repeated-measures ANOVAs with subjects as the random factor and sentence type and time (10 timepoints) as the fixed factors. For the first post hoc ANOVA, sentence type included 3 levels (plausible, implausible, and rotated) with results shown in the fifth column of Table 2. A region with a significant interaction of sentence type by time over the 3 sentence types was tested with a second ANOVA for a significant interaction by time over just the 2 intelligible sentence types (plausible and implausible) with results shown in the sixth column. In the seventh column, a region was assigned a stimulus preference for rotated speech if the greater response was evoked by spectrally rotated sentences. Likewise, if the response was greater for either plausible or implausible sentences, then this indicated a preference for normal speech. If the region's response differentiated between plausible and implausible sentences, then this latter distinction was refined to a stimulus preference for either plausible or implausible speech dependent on the larger response.

Many regions in both hemispheres differentiated between the 3 sentence types. None of the left hemisphere regions had a preference for rotated speech. In the right hemisphere, only the cerebellum (RCBI and RCBII) distinguished between plausible and implausible sentences. Comparing evoked responses of the 3 regions (LdpOp, LpSTS, and RCBI) to their contralateral homologs (second column, Figure 5), we see that only the RpSTS shows some separation of rotated speech from normal speech (i.e., plausible and implausible) but not nearly to the extent observed in the LpSTS.

In summary, many regions characterized by their leftward asymmetry in the resting-state global signal were preferential for semantic processing. The most important of these were the left dorsal pars opercularis, the LpSTS, and RCBI, which discriminated between stimuli at all levels tested. Contralateral homologs of these 3 regions failed to show a clear preference for semantic processing. Among leftward asymmetric regions, a trend was seen for the processing of words over numbers and normal over rotated speech. This was reversed for rightward asymmetric regions with a trend for numbers over words and rotated over normal speech.

Discussion

By simply examining the difference in spontaneous BOLD fluctuations between hemispheres without removing the global signal, we have identified many regions with a leftward asymmetry that are preferential for semantic processing and putative attention-related regions with a rightward asymmetry. The notion that hemispheric asymmetries are a mathematical necessity

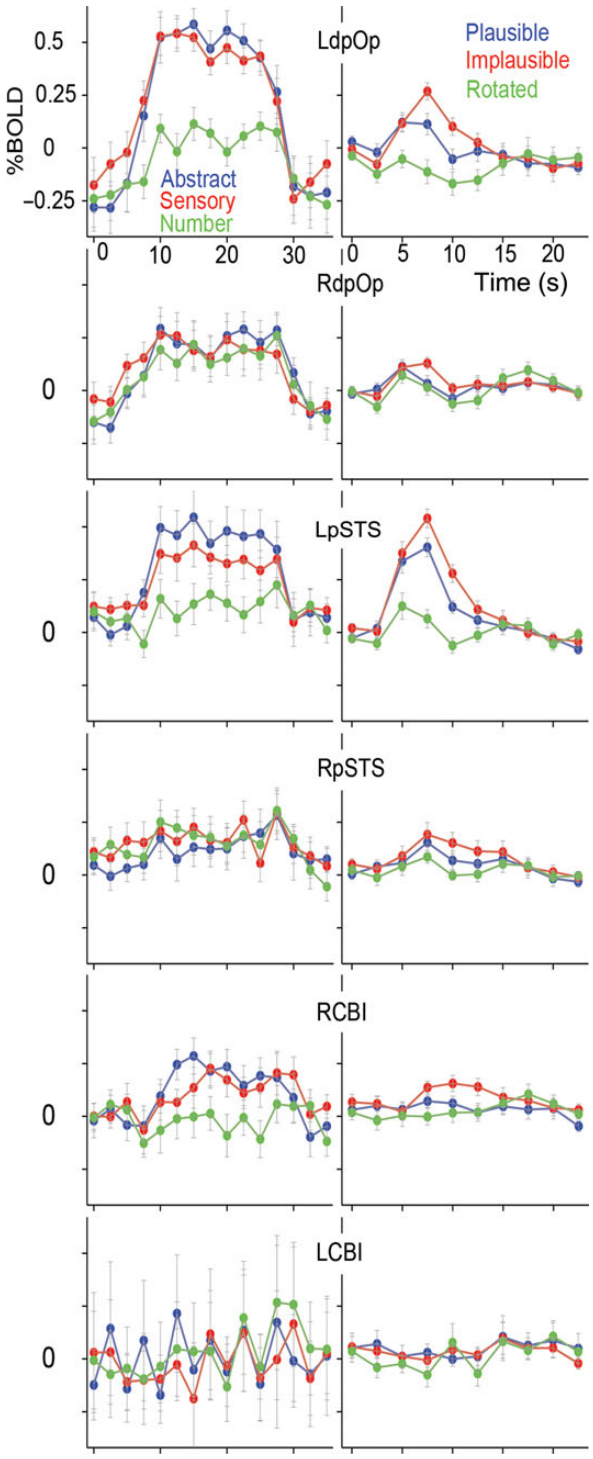

Figure 5. Subject averaged evoked BOLD responses for the 2 task-states. Regions LdpOp, LpSTS, and RCBI are identified in Figures 2 and 4*A* with coordinates provided in Table 1. Contralateral homologs RdpOp, RpSTS, and LCBI were created by taking the peak coordinate provided in Table 1, changing the sign of the *X* coordinate then drawing a 10-mm-diameter sphere at that point. Each row is a separate region including 2 regions along the inferior frontal gyrus (LdpOp and RdOp), 2 regions along the posterior superior temporal sulcus (LpSTS and RpSTS), and 2 lateral inferior cerebellar regions (RCBI and LCBI). The synonym and numerical magnitude judgment task is shown in the first column, and the sentence comprehension task is shown in the second column. The contralateral homologs fail to show the task differences present in the regions identified from their leftward asymmetry in the resting-state global signal.

that result from the left hemisphere confounding the right hemisphere (Frank 2000), and vice versa, is hard to reconcile with the leftward asymmetry found in the right cerebellum (Petersen et al. 1989; Fiez et al. 1992; Wang et al. 2013). To exempt this area, would be to ignore its well established involvement in language processing in the structural, lesion, and task-based neuroimaging research (Stoodley and Schmahmann 2009; Murdoch 2010; De Smet et al. 2013).

Although regions in the anterior temporal lobe (for reviews, see Patterson et al. 2007; Wong and Gallate 2012) failed to show a resting-state global signal hemispheric asymmetry in the smaller cohort of 20 subjects, a statistically significant leftward asymmetry was found in the larger cohort of 120 subjects (data not shown). A possible explanation for this discrepancy is the known BOLD signal loss from susceptibility artifacts in that part of the brain (Ojemann et al. 1997; Devlin et al. 2000); thus a larger number of subjects are needed to have the power to detect significant effects.

Our analysis of hemispheric asymmetries has provided only a static view of resting-state fluctuations. The brain not only lives in the present but remembers the past, so it may more accurately predict the future (Raichle 2010). Temporally, dynamic analyses that look over multiple time points such as the cross-covariance (e.g., McAvoy et al. 2012) are needed to unmask the full spatial extent of lateralization within the global signal.

Localization of Putative Language and Attention Preferential Areas in the Resting-State

The 2 most common methods to identify putative language and attention preferential regions from the brain's spontaneous fluctuations are functional connectivity (Biswal et al. 1995) and principal (PCA) or independent components analysis (ICA) (Beckmann et al. 2005). In functional connectivity, a seed region is correlated with all other voxels in the brain. The effectiveness of this technique is dependent on careful placement of the seed (Cohen et al. 2008). This method has the properties that homotopic voxels are strongly correlated with the seed and ipsilateral correlations are stronger than contralateral correlations (Gee et al. 2011). Studies that have regressed the global signal have struggled to identify language preferential (e.g., Zhao et al. 2011; Vogel et al. 2013) and attention preferential (e.g., Fox et al. 2006; Kucyi et al. 2012) networks. PCA and ICA parse the brain's spontaneous fluctuations into components that are either orthogonal or maximally separable, respectively, spatially, temporally or spatially and temporally. Putative language preferential areas are not limited to a single component, nor is a single component limited to language preferential areas (c.f. Smith et al. 2012). Identification of the relevant components requires either visual inspection or matching to a template (e.g., Smith et al. 2009). Moreover, language preferential regions are often represented symmetrically or with incomplete lateralization (Smith et al. 2009; Tie et al. 2014), and attention preferential regions appear bilaterally among several components with other regions (Damoiseaux et al. 2006; Smith et al. 2009).

Lesion, split–brain, and task fMRI studies have long established the left hemisphere dominance of language. Although the right hemisphere is neither "word deaf" or "word blind" (Sperry 1982), it has extremely limited syntactic, semantic, lexical, and phonological processing abilities despite being very capable at processing the contextual aspects of language (Gazzaniga 1983; Baynes et al. 1992; Bottini et al. 1994; Soroker et al. 2005). Furthermore, right hemisphere lesions produce deficits that are much more difficult to detect (Lindell 2006). Right hemisphere regions involved in language processing as identified by task-state fMRI are much less reliable and consistent across studies (Price 2010; Vigneau et al. 2011). Perhaps most dramatic are the brains of Broca's patients Leborgne and Lelong with their extensive left hemisphere damage and complete sparing of the right hemisphere (Dronkers et al. 2007). By comparing the intrinsic activity between hemispheres, we found that regions in left frontal and temporal cortex and the right cerebellum identified from their leftward asymmetry in the resting-state global signal replicated much of the known anatomy of language (Vigneau et al. 2006; Binder et al. 2009; Poeppel et al. 2012; Price 2012; Friederici and Gierhan 2013). By specifically identifying the lateralized organization of the resting-state global signal to semantic processing, we have sought to establish only an initial proof of principle. It has been posited that the right hemisphere has a dominant role in attention from observations of stroke patients with spatial neglect following right hemisphere lesions (Heilman and Abell 1980; Weintraub and Mesulam 1987; Ringman et al. 2004). In the absence of neglect, subjects with right hemisphere lesions have greater impairments in the contralesional hemispace during visual search tasks than subjects with left hemisphere lesions (Mapstone et al. 2003; Rabuffetti et al. 2012). In split-brain patients, the right hemisphere's performance of visuospatial tasks is superior to that of the left (for a review, see Gazzaniga 2000). We identified many areas long associated with attention in the right hemisphere, which displayed a rightward asymmetry including the TPJ and regions in frontal and parietal cortex (Pardo et al. 1991; Shulman et al. 2010; Cai et al. 2013; Kristensen et al. 2013).

Lateralization is a Fundamental Level of Organization in the Human Brain

The global signal has been a source of great controversy in resting-state fMRI. This debate concerns whether it should be considered a nuisance or confounding variable and how best to account for its contributions to the brain's spontaneous fluctuations (Macey et al. 2004; Murphy et al. 2008; Chang and Glover 2009; Fox et al. 2009; Anderson et al. 2011; Chai et al. 2012; Chen et al. 2012; He and Liu 2012; Saad et al. 2012; Falahpour et al. 2013; Keller et al. 2013). The global signal is typically regressed from the resting-state data before further analysis by a myriad of approaches including clustering (e.g., Salvador et al. 2005; Yeo et al. 2011), graph theory (e.g., Sporns and Honey 2006; Power et al. 2011), neural networks (e.g., Hacker et al. 2013), and modularity (e.g., Newman 2006; Ferrarini et al. 2009), among others. All these techniques seek to establish the functional organization of the brain. What insight that has been gained on the most venerable level of organization, lateralization, has focused on the residual lateralization present regionally after regression of the global signal (Liu et al. 2009; Gee et al. 2011; Wang et al. 2013). Lateralization as a global brain property has not been explored.

Implicit or subvocal speech is presumably a large part of most people's inner life (Cleland et al. 1963). Most of us are "talking to ourselves" or at least thinking using semantic representations during task performance and when resting (Binder et al. 1999). If this signal is lateralized, it may be argued that this alone could account for the observed global signal hemispheric asymmetries. However, the presence of this inner chatter fails to explain the lateralized organization of the right hemisphere, which does not mirror the left and lacks a semantic preference. Moreover, this inner chatter relies on semantic representations that have been ascribed to the default mode network (Binder et al. 2009; Binder and Desai 2011), yet the presence of strong

connectivity within regions of the default mode network (Shulman et al. 1997; Raichle et al. 2001) after global signal regression is one of the most notable and well-replicated findings in the fMRI resting-state literature (e.g., Fox et al. 2005). Another possibility is that hemispheric asymmetry mapping (HAM) reflects nothing more than lip and tongue motion; however, our right hemisphere map lacks the mouth representations clearly seen in the left hemisphere. We would expect the mouth region to appear bilaterally as this is a common finding in functional neuroimaging studies (e.g., Petersen et al. 1988; Brown et al. 2008; Grabski et al. 2012). The right hemisphere regions in dorsal and ventral precentral cortex identified by HAM displayed a rightward asymmetry and were not preferential for language processing.

Our results demonstrate that at least some part of the global signal contains neurally relevant information. Moreover, the lateralization embedded in the global signal suggests a fundamental hierarchy intrinsic to the brain, left hemisphere versus right hemisphere (Gazzaniga et al. 1962), which has been largely overlooked in resting-state functional neuroimaging (Johnston et al. 2008). These results provide insight regarding the presence of lateralization in the intrinsic brain activity of normal, healthy subjects. Our approach expands the reach of functional imaging studies of the human brain in health and disease.

Funding

This work was supported by the Mallinckrodt Institute of Radiology (MIR 12-023 and MRF 3618-92508 to M.M.); National Institutes of Health (NINDS NS080675 to M.E.R., NS061144 to S.E.P.), the McDonnell Foundation (Collaborative Action Award to S.E.P.), the Simons Foundation (Award 95177 to S.E.P.), and the Washington University Neuroimaging Informatics and Analysis Center led by Dan Marcus (5P30NS048056). Funding for 120 subject validation data set was provided by the National Institutes of Health (5R01 HD057076-S1 and R01HD057076 to Brad Schlaggar, K12 EY16336 to John Pruett, and K01DA027046 to Christina Lessov-Schlaggar), Barnes-Jewish Hospital Foundation (Christina Lessov-Schlaggar), McDonnell Center for Systems Neuroscience as Washington University (Christina Lessov-Schlaggar), Alvin J. Siteman Cancer Center (via NCI Cancer Center Support Grant P30 CA91842 to Christina Lessov-Schlaggar), and the Intellectual and Developmental Disabilities Research Center at Washington University (NIH/NICHD P30 HD062171).

Notes

We thank James Keidel for providing the uttered sentences; Marion Harris for facilities support; Linda Hood for help with the scanning; Avi Snyder, Evan Gordon, and Tim Laumann for helpful discussions, Binyam Nardos and Giovanni d'Avossa for help with the experimental design, and Fran Miezin for technical support. The 120 subject validation data set was provided courtesy of Brad Schlaggar, Christina Lessov-Schlaggar, Jessica Church, Joe Dubis, Eric Feczko, Katie Ihnen, Maital Neta, and Alecia Vogel. We thank the referees whose constructive criticisms greatly improved the quality of this manuscript. *Conflict of Interest*: None declared.

References

Algina J. 1997. Generalization of improved general approximation tests to split-plot designs with multiple between-subjects factors and/or multiple within-subjects factors. Br J Math Stat Psychology. 50:243–252.

Anderson JS, Druzgal TJ, Lopez-Larson M, Jeong E-K, Desai K, Yurgelun-Todd D. 2011. Network anticorrelations, global regression, and phase-shifted soft tissue correction. Hum Brain Mapp. 32:919–934.

Baynes K, Tramo MJ, Gazzaniga MS. 1992. Reading with a limited lexicon in the right hemisphere of a callosotomy patient. Neuropsychologia. 30:187–200.

Beckmann CF, DeLuca M, Devlin JT, Smith SM. 2005. Investigations into resting-state connectivity using independent component analysis. Philos Trans R Soc Lond B Biol Sci. 360:1001–1013.

Binder JR, Desai RH. 2011. The neurobiology of semantic memory. Trends Cogn Sci. 15:527–536.

Binder JR, Desai RH, Graves WW, Conant LL. 2009. Where is the semantic system? A critical review and meta-analysis of 120 functional neuroimaging studies. Cereb Cortex. 19:2767–2796.

Binder JR, Frost JA, Hammeke TA, Bellgowan PS, Rao SM, Cox RW. 1999. Conceptual processing during the conscious resting state. A functional MRI study. J Cogn Neurosci. 11:80–95.

Biswal B, Yetkin FZ, Haughton VM, Hyde JS. 1995. Functional connectivity in the motor cortex of resting human brain using echo-planar MRI. Magn Reson Med. 34:537–541.

Blesser B. 1972. Speech perception under conditions of spectral transformation: I. Phonetic characteristics. J Speech Hear Res. 15:5–41.

Bookheimer SY. 2002. New approaches to understanding the cortical organization of semantic processing. Annu Rev Neurosci. 25:151–188.

Bottini G, Corcoran R, Sterzi R, Paulesu E, Schenone P, Scarpa P, Frackowiak RSJ, Frith CD. 1994. The role of the right hemisphere in the interpretation of figurative aspects of language: a positron emission tomography activation study. Brain. 117:1241–1253.

Broca P. 1861. Perte de la parole: ramollissement chronique et destruction partielle du lobe anterieur gauche du cerveau. Bulletins de la Societe d'anthropologie, 1re serie. 2:235–238.

Brown S, Ngan E, Liotti M. 2008. A larynx area in the human motor cortex. Cereb Cortex. 18:837–845.

Cai Q, Van der Haegen L, Brysbaert M. 2013. Complementary hemispheric specialization for language production and visuospatial attention. Proc Natl Acad Sci USA. 110:E322–E330.

Carbonell F, Bellec P, Shmuel A. 2011. Global and system-specific resting-state fMRI fluctuations are uncorrelated: principal component analysis reveals anti-correlated networks. Brain Connect. 1:496–510.

Chai XJ, Castanon AN, Ongur D, Whitfield-Gabrieli S. 2012. Anticorrelations in resting state networks without global signal regression. Neuroimage. 59:1420–1428.

Chang C, Glover GH. 2009. Effects of model-based physiological noise correction on default mode network anti-correlations and correlations. Neuroimage. 47:1448–1459.

Chen G, Chen G, Xie C, Ward BD, Li W, Antuono P, Li S-J. 2012. A method to determine the necessity for global signal regression in resting-state fMRI studies. Magn Reson Med. 68:1828–1835.

Cleland DL, Davies WC, Davies TC. 1963. Research in reading. Read Teach. 16:224–228.

Cohen AL, Fair DA, Dosenbach NUF, Miezin FM, Dierker D, Van Essen DC, Schlaggar BL, Petersen SE. 2008. Defining functional areas in individual human brains using resting functional connectivity MRI. Neuroimage. 41:45–57.

Cohen L, Dahaene S. 2004. Specialization within the ventral stream: the case for the visual word from area. Neuroimage. 22:466–476.

Corbetta M, Shulman GL. 2011. Spatial neglect and attention networks. Annu Rev Neurosci. 34:569–599.

Coughlan AK, Warrington EK. 1978. Word-comprehension and word-retrieval in patients with localized cerebral lesions. Brain. 101:163–185.

Damasio H, Tranel D, Grabowski T, Adolphs R, Damasio A. 2004. Neural systems behind word and concept retrieval. Cognition. 92:179–229.

Damoiseaux JS, Rombouts SA, Barkhof F, Scheltens P, Stam CJ, Smith SM, Beckmann CF. 2006. Consistent resting-state networks across healthy subjects. Proc Natl Acad Sci USA. 103:13848–13853.

Daselaar SM, Huijbers W, Eklund K, Moscovitch M, Cabeza R. 2013. Resting-state functional connectivity of ventral parietal regions associated with attention reorienting and episodic recollection. Front Hum Neurosci. 7:1–9.

De Smet HJ, Paquier P, Verhoeven J, Marien P. 2013. The cerebellum: its role in language and related cognitive and affective functions. Brain Lang. 127:334–342.

Devlin JT, Russell RP, Davis MH, Price CJ, Wilson J, Moss HE, Matthews PM, Tyler LK. 2000. Susceptibility-induced loss of signal: comparing PET and fMRI on a semantic task. Neuroimage. 11:589–600.

Dronkers NF, Plaisant O, Iba-Zizen MT, Cabanis EA. 2007. Paul Broca's historic cases: high resolution MR imaging of the brains of Leborgne and Lelong. Brain. 130:1432–1441.

Duerden EG, Arsalidou M, Lee MH, Taylor MJ. 2013. Lateralization of affective processing in the insula. Neuroimage. 78:159–175.

Falahpour M, Refai H, Bodurka J. 2013. Subject specific BOLD fMRI respiratory and cardiac response functions obtained from global signal. Neuroimage. 72:252–264.

Ferrarini L, Veer IM, Baerends E, van Tol MJ, Renken RJ, van der Wee NJ, Veltman DJ, Aleman A, Zitman FG, Penninx BWJH, et al. 2009. Hierarchical functional modularity in the resting-state human brain. Hum Brain Mapp. 30:2220–2231.

Fiez JA, Petersen SE, Cheney MK, Raichle ME. 1992. Impaired non-motor learning and error detection associated with cerebellar damage. A single case study. Brain. 115(Pt 1):155–178.

Forman SD, Cohen JD, Fitzgerald M, Eddy WF, Mintun MA, Noll DC. 1995. Improved assessment of significant activation in functional magnetic resonance imaging (fMRI): use of a cluster-size threshold. Magn Reson Med. 33:636–647.

Fox MD, Corbetta M, Snyder AZ, Vincent JL, Raichle ME. 2006. Spontaneous neuronal activity distinguishes human dorsal and ventral attention systems. Proc Natl Acad Sci USA. 103:10046–10051.

Fox MD, Snyder AZ, Vincent JL, Corbetta M, Van Essen DC, Raichle ME. 2005. The human brain is intrinsically organized into dynamic, anticorrelated functional networks. Proc Natl Acad Sci USA. 102:9673–9678.

Fox MD, Zhang D, Snyder AZ, Raichle ME. 2009. The global signal and observed anticorrelated resting state brain networks. J Neurophysiol. 101:3270–3283.

Frank KA. 2000. Impact of a confounding variable on a regression coefficient. Soc Methods Res. 29:147–194.

Friederici AD, Gierhan SME. 2013. The language network. Curr Opin Neurobiol. 23:250–254.

Friston KJ, Holmes AP, Poline JB, Grasby PJ, Williams SC, Frackowiak RS, Turner R. 1995. Analysis of fMRI time-series revisited. Neuroimage. 2:43–53.

Friston KJ, Williams S, Howard R, Frackowiak RS, Turner R. 1996. Movement-related effects in fMRI time-series. Magn Reson Med. 35:346–355.

Gazzaniga MS. 1983. Right hemisphere language following brain bisection: a 20-year perspective. Am Psychol. 38:525–537.

Gazzaniga MS. 2000. Cerebral specialization and interhemispheric communication: does the corpus callosum enable the human condition? Brain. 123(Pt 7):1293–1326.

Gazzaniga MS, Bogen JE, Sperry RW. 1962. Some functional effects of sectioning the cerebral commissures in man. Proc Natl Acad Sci USA. 48:1765–1769.

Gee DG, Biswal BB, Kelly C, Stark DE, Marguiles DS, Shehzad Z, Uddin LQ, Klein DF, Banich MT, Castellanos FX, et al. 2011. Low frequency fluctuations reveal integrated and segregated processing among the cerebral hemispheres. Neuroimage. 54:517–527.

Grabski K, Lamalle L, Vilain C, Schwartz J-L, Vallee N, Tropres I, Baciu M, Le Bas J-F, Sato M. 2012. Functional MRI assessment of orofacial articulators: neural correlates of lip, jaw, larynx, and tongue movements. Hum Brain Mapp. 33:2306–2321.

Greicius MD, Krasnow B, Reiss AL, Menon V. 2003. Functional connectivity in the resting brain: a network analysis of the default mode hypothesis. Proc Natl Acad Sci USA. 100:253–258.

Hacker CD, Laumann TO, Szrama NP, Baldassarre A, Snyder AZ, Leuthardt EC, Corbetta M. 2013. Resting state network estimation in individual subjects. NeuroImage. 82:616–633.

Hampson M, Petersen BS, Skudlarski P, Gatenby JC, Gore JC. 2002. Detection of functional connectivity using temporal correlations in MR images. Hum Brain Mapp. 15:247–262.

He H, Liu TT. 2012. A geometric view of global signal confounds in resting-state functional MRI. Neuroimage. 59:2239–2348.

Heilman KM, Abell TVD. 1980. Right hemisphere dominance for attention. Neurology. 30:327–330.

Hutchison RM, Gallivan JP, Culham JC, Gati JS, Menon RS, Everling S. 2012. Functional connectivity of the frontal eye fields in humans and macaque monkeys investigated with resting-state fMRI. J Neurophysiol. 107:2463–2474.

Jefferies E, Patterson K, Jones RW, Ralph MAL. 2009. Comprehension of concrete and abstract words in semantic dementia. Neuropsychology. 23:492–499.

Johnston JM, Vaishnavi SN, Smyth MD, Zhang D, He BJ, Zempel JM, Shimony JS, Snyder AZ, Raichle ME. 2008. Loss of resting interhemispheric functional connectivity after complete section of the corpus callosum. J Neurosci. 28:6453–6458.

Keller CJ, Bickel S, Honey CJ, Groppe DM, Entz L, Craddock RC, Lado FA, Kelly C, Milham M, Mehta AD. 2013. Neurophysiological investigation of spontaneous correlated and anticorrelated fluctuations of the BOLD signal. J Neurosci. 33:6333–6342.

Keller SS, Crow T, Foundas A, Amunts K, Roberts N. 2009. Broca's area: nomenclature, anatomy, typology and asymmetry. Brain Lang. 109:29–48.

Keppel G. 1991. Design and Analysis, A Researcher's Handbook. Third Edition. Upper Saddle River: Prentice Hall.

Kristensen LB, Wang L, Petersson KM, Hagoort P. 2013. The interface between language and attention: prosodic focus marking recruits a general attention network in spoken language comprehension. Cereb Cortex. 23:1836–1848.

Kucyi A, Hodaie M, Davis KD. 2012. Lateralization in intrinsic functional connectivity of the temporoparietal junction with salience- and attention-related brain networks. J Neurophysiol. 108:3382–3392.

Lambon Ralph MA, Probic G, Jefferies E. 2009. Conceptual knowledge is underpinned by the temporal pole bilaterally: convergent evidence from rTMS. Cereb Cortex. 19:832–838.

LeDoux JE, Wilson DH, Gazzaniga MS. 1977. Manipulo-spatial aspects of cerebral lateralization: clues to the origin of lateralization. Neuropsychologia. 15:743–750.

Lee MH, Hacker CD, Snyder AZ, Corbetta M, Zhang D, Leuthardt EC, Shimony JS. 2012. Clustering of resting state networks. PLoS One. 7:e40370.

Lindell AK. 2006. In your right mind: right hemisphere contributions to language processing and production. Neuropsychol Rev. 16:131–148.

Liu H, Stufflebeam SM, Sepulcre J, Hedden T, Buckner RL. 2009. Evidence from intrinsic activity that asymmetry of the human brain is controlled by multiple factors. Proc Natl Acad Sci USA. 106:20499–20503.

Lowe MJ, Mock BJ, Sorenson JA. 1998. Functional connectivity in single and multislice echoplanar imaging using resting-state fluctuations. Neuroimage. 7:119–132.

Macey PM, Macey KE, Kumar R, Harper RM. 2004. A method for removal of global effects from fMRI time series. Neuroimage. 22:360–366.

Mapstone M, Weintraub S, Nowinski C, Kaptanoglu G, Gitelman DR, Mesulam MM. 2003. Cerebral hemispheric specialization for spatial attention: spatial distribution of search-related eye fixations in the absence of neglect. Neuropsychologia. 41:1396–1409.

Markett S, Reuter M, Montag C, Voigt G, Lachmann B, Rudorf S, Elger CE, Weber B. 2014. Assessing the function of the fronto-parietal attention network: insights from resting-state fMRI and the attentional network test. Hum Brain Mapp. 35:1700–1709.

McAvoy M, Larson-Prior L, Ludwikow M, Zhang D, Snyder AZ, Gusnard DA, Raichle ME, d'Avossa G. 2012. Dissociated mean and functional connectivity BOLD signals in visual cortex during eyes closed and fixation. J Neurophysiol. 108:2363–2372.

McAvoy M, Larson-Prior L, Nolan TS, Vaishnavi SN, Raichle ME, d'Avossa G. 2008. Resting states affect spontaneous BOLD oscillations in sensory and paralimbic cortex. J Neurophysiol. 100:922–931.

McAvoy MP, Ollinger JM, Buckner RL. 2001. Cluster size thresholds for assessment of significant activation in fMRI. Neuroimage. 13:S198.

Muller AM, Meyer M. 2014. Language in the brain at rest: new insights from resting state data and graph theoretical analysis. Front Hum Neurosci. 8:228.

Murdoch BE. 2010. The cerebellum and language: historical perspective and review. Cortex. 46:858–868.

Murphy K, Birn RM, Handwerker DA, Jones TB, Bandettini PA. 2008. The impact of global signal regression on resting state correlations: are anti-correlated networks introduced? Neuroimage. 29:740–750.

Newman MEJ. 2006. Modularity and community structure in networks. Proc Natl Acad Sci USA. 103:8577–8582.

Noppeney U, Price CJ. 2004. Retrieval of abstract semantics. Neuroimage. 22:164–170.

Ojemann JG, Akbudak E, Snyder AZ, McKinstry RC, Raichle ME, Conturo TE. 1997. Anatomic localization and quantitative analysis of gradient refocused echo-planar fMRI susceptibility artifacts. Neuroimage. 6:156–167.

Pardo JV, Fox PT, Raichle ME. 1991. Localization of a human system for sustained attention by positron emission tomography. Nature. 349:61–64.

Patterson K, Nestor PJ, Rogers TT. 2007. Where do you know what you know? The representation of semantic knowledge in the human brain. Nat Rev Neurol. 8:976–987.

Petersen SE, Fox PT, Posner MI, Mintun M, Raichle ME. 1988. Positron emission tomographic studies of the cortical anatomy of single-word processing. Nature. 331:585–589.

Petersen SE, Fox PT, Posner MI, Mintun M, Raichle ME. 1989. Positron emission tomographic studies of the processing of single words. J Cognitive Neurosci. 1:153–170.

Petersen SE, Fox PT, Snyder AZ, Raichle ME. 1990. Activation of extrastriate and frontal cortical areas by visual words and word-like stimuli. Science. 249:1041–1044.

Poeppel D, Emmorey K, Hickok G, Pylkkanen L. 2012. Towards a new neurobiology of language. J Neurosci. 32:14125–14131.

Power JD, Barnes KA, Snyder AZ, Schlaggar BL, Petersen SE. 2012. Spurious but systematic correlations in functional connectivity MRI networks arise from subject motion. Neuroimage. 59:2142–2154.

Power JD, Cohen AL, Nelson SM, Wig GS, Barnes KA, Church JA, Vogel AC, Laumann TO, Miezin FM, Schlaggar BL, et al. 2011. Functional network organization of the human brain. Neuron. 72:665–678.

Power JD, Mitra A, Laumann TO, Snyder AZ, Schlaggar BL, Petersen SE. 2014. Methods to detect, characterize, and remove motion artifact in resting state fMRI. Neuroimage. 84:320–341.

Power JD, Schlaggar BL, Lessov-Schlaggar CN, Petersen SE. 2013. Evidence for hubs in human functional brain networks. Neuron. 79:798–813.

Price CJ. 2010. The anatomy of language: a review of 100 fMRI studies published in 2009. Ann N Y Acad Sci. 1191:62–88.

Price CJ. 2012. A review and synthesis of the first 20 years of PET and fMRI studies of heard speech, spoken language and reading. Neuroimage. 62:816–847.

Rabuffetti M, Farina E, Alberoni M, Pellegatta D, Ildebrando A, Affanni P, Forni M, Ferrarin M. 2012. Spatio-temporal features of visual exploration in unilaterally brain-damaged subjects with or without neglect: results from a touchscreen test. PLoS ONE. 7:e31511.

Raichle ME. 2010. Two views of brain function. Trends Cogn Sci. 14:180–190.

Raichle ME, MacLeod AM, Snyder AZ, Powers WJ, Gusnard DA, Shulman GL. 2001. A default mode of brain function. Proc Natl Acad Sci USA. 98:676–682.

Ringman JM, Saver JL, Woolson RF, Clarke WR, Adams HP. 2004. Frequency, risk factors, anatomy, and course of unilateral neglect in an acute stroke cohort. Neurology. 63:468–474.

Rowland DJ, Garbow JR, Laforest R, Snyder AZ. 2005. Registration of [18F]FDG microPET and small-animal MRI. Nucl Med Biol. 32:567–572.

Saad ZS, Gotts SJ, Murphy K, Chen G, Jo HJ, Martin A, Cox RW. 2012. Trouble at rest: how correlation patterns and group differences become distorted after global signal regression. Brain Connect. 2:25–32.

Salvador R, Suckling J, Coleman MR, Pickard JD, Menon D, Bullmore E. 2005. Neurophysiological architecture of functional magnetic resonance images of human brain. Cereb Cortex. 15:1332–1342.

Satterthwaite TD, Elliott MA, Gerraty RT, Ruparel K, Loughead J, Calkins ME, Eickhoff SB, Hakonarson H, Gur RC, Gur RE, et al. 2013. An improved framework for confound regression and filtering for control of motion artifact in the preprocessing of resting-state functional connectivity data. Neuroimage. 64:240–256.

Scholvinck ML, Maier A, Ye FQ, Duyn JH, Leopold DA. 2010. Neural basis of global resting-state fMRI activity. Proc Natl Acad Sci USA. 107:10238–10243.

Scott SK, Blank CC, Rosen S, Wise RJS. 2000. Identification of a pathway for intelligible speech in the left temporal lobe. Brain. 123:2400–2406.

Shmueli K, van Gelderen P, de Zwart JA, Horovitz SG, Fukunaga M, Jansma JM, Duyn JH. 2007. Low-frequency fluctuations in the cardiac rate as a source of variance in the resting-state fMRI BOLD signal. Neuroimage. 38:306–320.

Shulman GL, Fiez JA, Corbetta M, Buckner RL, Miezin FM, Raichle ME, Petersen SE. 1997. Common blood flow changes across visual tasks: II. Decreases in cerebral cortex. J Cogn Neurosci. 9:648–663.

Shulman GL, Pope DL, Astafiev SV, McAvoy MP, Snyder AZ, Corbetta M. 2010. Right hemisphere dominance during spatial selective attention and target detection occurs outside the dorsal frontoparietal network. J Neurosci. 30:3640–3651.

Smith SM, Fox PT, Miller KL, Glahn DC, Fox PM, Mackay CE, Filippini N, Watkins KE, Toro R, Laird AR, et al. 2009. Correspondence of the brain's functional architecture during activation and rest. Proc Natl Acad Sci USA. 106:13040–13045.

Smith SM, Miller KL, Moeller S, Xu J, Auerbach EJ, Woolrich MW, Beckmann CF, Jenkinson M, Andersson J, Glasser MF, et al. 2012. Temporally-independent functional modes of spontaneous brain activity. Proc Natl Acad Sci USA. 109:3131–3136.

Soroker N, Kasher A, Giora R, Batori G, Corn C, Gil N, Zaidel E. 2005. Processing of basic speech acts following localized brain damage: a new ligt on the neuroanatomy of language. Brain Cogn. 57:214–217.

Sperry R. 1982. Some effects of disconnecting the cerebral hemispheres. Science. 217:1223–1226.

Sporns O, Honey CJ. 2006. Small worlds inside big brains. Proc Natl Acad Sci USA. 103:19219–19220.

Stoodley CJ, Schmahmann JD. 2009. Functional topography in the human cerebellum: a meta-analysis of neuroimaging studies. Neuroimage. 44:489–501.

Talairach J, Tournoux P. 1988. Co-Planar Stereotaxic Atlas of the Human Brain. New York: Thieme Medical Publishers, Inc.

Tie Y, Rigolo L, Norton IH, Huang RY, Wu W, Orringer O, Mukundan S Jr, Golby AJ. 2014. Defining language networks from resting-state fMRI for surgical planning—a feasibility study. Hum Brain Mapp. 35:1018–1030.

Tomasi D, Volkow ND. 2012. Resting functional connectivity of language networks: characterization and reproducibility. Mol Psychiatr. 17:841–854.

Vigneau M, Beaucousin V, Herve PY, Duffau H, Crivello F, Houde O, Mazoyer B, Tzourio-Mazoyer N. 2006. Meta-analyzing left hemisphere language areas: phonology, semantics, and sentence processing. Neuroimage. 30:1414–1432.

Vigneau M, Beaucousin V, Herve P-Y, Jobard G, Petit L, Crivello F, Mellet E, Zago L, Mazoyer B, Tzourio-Mazoyer N. 2011. What is the right-hemisphere contribution to phonological, lexico-semantic, and sentence processing? Insights from a meta-analysis. Neuroimage. 54:577–593.

Vogel AC, Church JA, Power JD, Miezin FM, Petersen SE, Schlaggar BL. 2013. Functional network architecture of reading-related regions across development. Brain Lang. 125:231–243.

Vossel S, Geng JJ, Fink GR. 2014. Dorsal and ventral attention systems: distinct neural circuits but collaborative roles. Neuroscientist. 20:150–159.

Wang D, Buckner RL, Liiu H. 2013. Cerebellar asymmetry and its relation to cerebral asymmetry estimated by intrinsic functional connectivity. J Neurophysiol. 109:46–57.

Warrington EK, McKenna P, Orpwood L. 1998. Single word comprehension: a concrete and abstract word synonym test. Neuropsychol Rehabil. 8:143–154.

Weintraub S, Mesulam MM. 1987. Right cerebral dominance in spatial attention. Further evidence based on ipsilateral neglect. Arch Neurol. 44:621–625.

Weissenbacher A, Kasess C, Gerstl F, Lazenberger R, Moser E, Windischberger C. 2009. Correlations and anticorrelations in resting-state functional connectivity MRI: a quantitative comparison of preprocessing strategies. Neuroimage. 47:1408–1416.

Wernicke C. 1874. Der Aphasische Symptomencomplex. Breslau: Cohn and Weigert.

Wise RG, Ide K, Poulin MJ, Tracey I. 2004. Resting fluctuations in arterial carbon dioxide induce significant low frequency variations in BOLD signal. Neuroimage. 21:1652–1664.

Wise RJS, Scott SK, Blank SC, Mummery CJ, Murphy K, Warburton EA. 2001. Separate neural subsystems within 'Wernicke's area'. Brain. 124:83–95.

Wong C, Gallate J. 2012. The function of the anterior temporal lobe: a review of the empirical evidence. Brain Res. 1449:94–116.

Yan CG, Cheung B, Kelly C, Colcombe S, Craddock RC, Di Martino A, Li Q, Zuo XN, Castellanos FX, Milham MP. 2013. A comprehensive assessment of regional variation in the impact of head micromovements of functional connectomics. Neuroimage. 76:183–201.

Yeo BT, Krienen FM, Sepulcre J, Sabuncu MR, Lashkari D, Hollinshead M, Roffman JL, Smoller JW, Zollei L, Polimeni JR, et al. 2011. The organization of the human cerebral cortex estimated by intrinsic functional connectivity. J Neurophysiol. 106:1125–1165.

Zeng L-L, Wang D, Fox MD, Sabuncu M, Hu D, Ge M, Buckner RL, Liu H. 2014. Neurobiological basis of head motion in brain imaging. Proc Natl Acad Sci USA. 111:6058–6062.

Zhao J, Liu J, Li J, Liang J, Feng L, Ai L, Lee K, Tian J. 2011. Intrinsically organized network for word processing during the resting state. Neurosci Lett. 487:27–31.

Zhu L, Fan Y, Zou Q, Wang J, Gao J-H, Niu Z. 2014. Temporal reliability and lateralization of the resting-state language network. PLOS One. 9:e85880.